Resonance Raman Characterization of Reaction Centers in Which Bacteriochlorophyll Replaces the Photoactive Bacteriopheophytin†

Kazimierz Czarnecki,‡ Craig C. Schenck,§ and David F. Bocian*,‡

Department of Chemistry, University of California, Riverside, California 92521, and Department of Biochemistry, Colorado State University, Fort Collins, Colorado 80523

Received July 2, 1997; Revised Manuscript Received September 11, 1997⊗

ABSTRACT: Q_y-excitation resonance Raman (RR) spectra are reported for two mutant reactions centers (RCs) from *Rhodobacter sphaeroides* in which the photoactive bacteriopheophytin (BPh_L) is replaced by a bacteriochlorophyll (BChl) molecule, designated by β_L. One mutation, (M)L214H, yields the pigment change via introduction of a histidine residue at position M214. The other mutation, (M)L214H/(L)-E104V, removes the putative hydrogen bond between β_L and the native glutamic acid residue at position L104. The vibrational signatures of the β_L cofactors of the mutants are compared with one another and with those of the accessory BChls ($BChl_{L,M}$) in both β-mutant and wild-type RCs. The spectroscopic data reveal the following: (1) The β_L cofactor is a five-coordinate BChl molecule with a histidine axial ligand. The conformation of β_L and the strength of the Mg−histidine bond are very similar to that of $BChl_{L,M}$. (2) The β_L cofactor is oriented in the protein pocket in a manner similar to that of BPh_L of wild-type. (3) The β_L cofactor of the (M)L214H mutant forms a hydrogen bond with glutamic acid L104 via the C_9-keto group of the macrocycle. The strength of this hydrogen bond is identical to that formed between this protein residue and the C_9-keto group of BPh_L in wild-type. (4) The hydrogen bonding interaction at the C_9-keto site induces secondary cofactor−protein interactions which involve the C_{2a}-acetyl and C_b-alkyl substituent groups. Collectively, the vibrational signatures of β_L indicate that its intrinsic physicochemical properties are very similar to those of $BChl_L$. Consequently, the initial charge-separated intermediate in β-type RCs is best characterized as a thermal/quantum mechanical admixture of $P^+\beta_L^-$ and $P^+BChl_L^-$ (P is the primary electron donor), as originally proposed by Kirmaier et al. [(1995) *J. Phys. Chem. 99,* 8903−8909].

The reaction center (RC)[1] is a membrane-bound protein responsible for the initial charge-separation process in photosynthesis (*1*−*6*). Bacterial RCs consist of four bacteriochlorophylls (BChls), two bacteriopheophytins (BPhs), and four other nontetrapyrrolic cofactors arranged in three polypeptide subunits designated by L, M, and H. The primary electron donor in RCs is a dimer of BChls, designated the special pair or P. The first electron-transfer intermediate which accumulates to a substantial population is the anion radical of the BPh cofactor in the L subunit (*1*−*6*). The X-ray crystal structures of RCs from two different purple bacteria (*Rhodobacter sphaeroides* and *Rhodopseudomonas viridis*) reveal that P, the accessory BChls, and the BPhs are arranged in the L and M subunits such that the macroscopic symmetry is approximately C_2 (*7*−*15*). The Mg(II) ions of the two BChls in P and the two accessory BChls are each ligated to a histidine residue of the protein (*8*, *9*). This ligation conserves the approximate C_2 symmetry in the RC. This symmetry is broken, however, by inequivalences at other positions of the primary amino acid sequence of the L versus M subunits.

One of the most unusual aspects of the electron-transfer process in RCs is that it is unidirectional, proceeding only down the L branch (*16*). This unidirectionality is presumably dictated by the asymmetrical distribution of amino acid residues in the L versus M branches. The possibility that certain protein residues might be responsible for unidirectional electron transfer has led to the construction of a variety of genetically modified RCs in which the L- versus M-side asymmetries are altered (*17*). β-Type RCs constitute one general class of these mutants (*18*, *19*). In these RCs, a histidine residue is placed over the face of the primary electron acceptor (BPh_L in wild-type RCs). This replacement results in incorporation of a BChl (designated β_L) rather than a BPh into the acceptor site. [Altered cofactor composition in RCs can also be accomplished via chemical modification or exchange techniques (*20*).] The BChl molecule differs from BPh only in that a Mg(II) ion replaces the two central protons. The histidine residue presumably serves as an axial ligand to β_L and selects for incorporation of the Mg-containing pigment. However, the actual ligation state of β_L has not been determined. Although the driving force for initial electron transfer in the β-type RCs is significantly reduced owing to the more negative reduction potential of BChl versus BPh (*21*), the cofactor change does not lead to electron transfer to the normally inactive BPh_M or to blocked photochemistry (*18*, *19*, *22*−*24*).

† This work was supported by the National Institute of General Medical Sciences [Grants GM39781 (D.F.B.) and GM48245 (C.C.S.) and Research Career Development Award GM00536 (C.C.S.)] and the Colorado Agricultural Experiment Station [Grant 632 (C.C.S.)].

‡ University of California.

§ Colorado State University.

⊗ Abstract published in *Advance ACS Abstracts,* November 15, 1997.

[1] Abbreviations: BChl, bacteriochlorophyll; BPh, bacteriopheophytin; L, M, and H, light, medium, and heavy polypeptides of the reaction center; P, the special pair primary electron donor; RCs, reaction centers; RR, resonance Raman; SERDS, shifted-excitation Raman difference spectroscopy.

S0006-2960(97)01600-0 CCC: $14.00

The photochemical behavior of the β-type RCs is dictated by the detailed properties of the initial charge-separated intermediate. These properties have been investigated in detail by Kirmaier et al. (*22*, *23*). Spectroscopic studies of β-type RCs reveal that the first intermediate contains $P^+\beta_L^-$. However, the angle between the transition dipole moments of the optical transitions of P and the anion is rotated by ~20° compared with that observed for the transitions of P and BPh_L^- in wild-type RCs (*22*). One possible explanation for this observation is that β_L is rotated in the protein pocket and/or assumes a very different structure from a typical BChl molecule. This interpretation does not appear to be consistent with preliminary X-ray crystallographic data for (M)L214H β-mutant RCs from *Rb. sphaeroides* (*25*). However, the resolution of this data is relatively low (3.3 Å) and the detailed orientation/structure of β_L cannot be assessed with certainty. An alternative explanation, favored by Kirmaier et al., which accounts for the various spectroscopic signatures of the initial charge-separated intermediate is that this species is a thermal/quantum admixture of $P^+\beta_L^-$ and $P^+BChl_L^-$ (*22*, *23*). The complicated nature of the intermediate has led these workers to designate this species as P^+I^-.

In order to fully elucidate the nature of P^+I^- in β-type RCs, it is necessary to have a clear picture of both the structure of β_L and its orientation in the protein pocket. The characterization of β_L is additionally important because a double mutant, wherein the second replacement is an aspartic acid placed near the accessory BChl on the active branch ($BChl_L$) in a β-type background, has been shown exhibit electron transfer down the normally inactive M branch of the RC (*26*). As noted above, the resolution of the currently available X-ray crystallographic data is not sufficient to elucidate the detailed structural characteristics of β_L (*25*). Vibrational spectroscopy and, in particular, resonance Raman (RR) spectroscopy provides attractive alternative for addressing these issues. The vibrational signatures of the ring-skeletal, carbonyl, and substituent modes reflect the conformation of the BChl macrocycle, the number and nature of the axial ligands to the Mg(II) ion, and the nature of the interactions between the substituent groups and the protein matrix (*27*−*47*). To date RR techniques have not been used to examine β-type RCs.

In this paper, we report RR studies of β-type RCs from *Rb. sphaeroides*. The RCs examined include the (M)L214H single mutant and (M)L214H/(L)E104V double mutant. In the latter mutant, the L104 glutamic acid residue, which is known to form a hydrogen bond with the C_9-keto group of the BPh_L in wild-type RCs (*8*,*9*,*28*−*30*), is replaced with a non-hydrogen-bonding residue. The examination of this mutant affords the opportunity to determine whether β_L is appropriately positioned in the protein pocket to form an equivalent hydrogen bond. All of the RR data were acquired using excitation into the red-most Q_y absorption bands of the cofactors. Q_y-excitation was chosen because these absorption features of the different cofactors are energetically better resolved than the Q_x or B absorptions, thus affording better selectivity in the acquisition of RR data for the individual pigments (*30*, *38*, *39*, *47*−*49*). The RR spectral features of β_L were compared with those of the accessory BChls in wild-type RCs and with these cofactors in the single and double β-mutant RCs. The spectral features of the accessory BChls (at least in wild-type RCs) are identical to one another (*38*, *46*, *49*) and identical to those of BChl in solution (*38*). Accordingly, these cofactors serve as benchmarks for the structural characteristics of typical BChl molecules. Collectively, the RR data provide further insights into structure, axial ligation, and site orientation of β_L and how these factors influence the photochemical characteristics of β-type RCs.

MATERIALS AND METHODS

The wild-type (strain WS231), (M)L214H mutant, and (M)L214H/(L)E104V mutant RCs were prepared, isolated, and purified as previously described (*18*, *22*, *50*). The RCs were solublized in 10 mM Tris-HCl (pH 8)/0.015% Triton X-100/1 mM EDTA. The quinone-reduced RCs were prepared by adding a slight excess of sodium dithionite to the sample.

The RR measurements were made on optically dense (OD ~1.8/mm at 800 nm; RC concentration ~63 mM), snowy samples at 25 K contained in 1 mm i.d. capillary tubes. The advantages and disadvantages of using snowy versus glassy samples have been previously discussed (*47*). Temperature control was achieved by mounting the sample on a cold tip of a closed cycle refrigeration system (ADP Cryogenics, DE-202 Displex).

The RR spectra were obtained using a red-optimized triple spectrograph and detection system that has been previously described (*38*). A Ti:sapphire laser (Coherent 890) pumped by an Ar ion laser (Coherent Innova 400−15UV) served as the excitation source. The laser powers were typically 1.5 mW. The power density on the sample was lowered by defocusing the incident beam. The resulting photon fluxes (~100 photons s^{-1} RC^{-1}) were low enough that only a few percent of the RCs exist in photogenerated transient states. In order to enhance the longevity of the samples, the capillary tubes were repositioned in the laser beam after every scan. The high-frequency (>1300 cm^{-1}) RR data sets for both β_L and the accessory BChls were obtained with 3 h of signal averaging (β_L, 180 × 60 s scans; accessory BChls, 360 × 30 s scans). The mid- and low-frequency (<1300 cm^{-1}) RR data sets of β_L were obtained with 4 h of signal averaging (120 × 120 s scans), while those of the accessory BChls were obtained with 2 h of signal averaging (60 × 120 s scans). Cosmic spikes in the individual scans were removed prior to coaddition of the scans. The spectral resolution was ~2 cm^{-1} in all spectral regions. The spectral data were calibrated using the known frequencies of fenchone (*51*).

The Q_y-excitation RR spectra observed for the wild-type, (M)L214H, and (M)L214H/(L)E104V RCs in the mid- and low-frequency regions (<1300 cm^{-1}) were essentially free from interference from fluorescence. As a consequence, the RR signals were readily observed in the absence of background corrections. In contrast, the RR spectra observed for all three RCs in the high-frequency region (>1300 cm^{-1}) were superimposed on an emission background. This characteristic of the spectra, in conjunction with the fact that the Q_y-excitation RR intensities of the high-frequency modes of BChl are generally lower than those of the mid- and low-frequency modes (*48*, *49*), compromised the quality of the spectra. [The pattern of strong mid/low- and weak high-frequency modes is a general characteristic of the Q_y-excitation RR spectra of BChl and is not specific to BChl in RCs (*52*).] Therefore, all of the high-frequency RR spectra were acquired using the shifted-excitation Raman difference

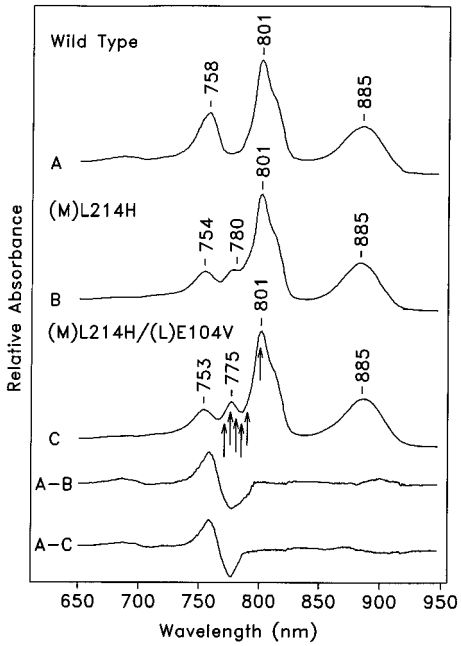

FIGURE 1: Low-temperature (10 K) near-infrared absorption spectra of wild-type (WS231), (M)L214H, and (M)L214H/(L)E104V RCs. The absorption difference spectra (wild-type−mutant) are shown in the lower two traces. The arrows in the spectrum of the (M)-L214H/(L)E104V RC mark the different excitation wavelengths used to acquire RR spectra.

spectroscopic (SERDS) technique (*48*, *53*). The application of the SERDS method to RCs has been previously discussed in detail (*39*, *40*, *47*−*49*). Briefly, data sets are acquired at two excitation wavelengths which differ by small wavenumber increments (typically 10 cm^{-1}). [The 3 h data acquisition times indicated above are for each of the two data sets required to construct SERDS traces]. These data sets are subtracted to yield a background-free RR difference (SERDS) spectrum. The difference spectra presented herein were obtained by subtracting the initial spectrum from the shifted spectrum. The spectral window is defined by the initial spectrum and corresponds to the wavenumber axis shown in the figures. The normal RR spectrum is then reconstructed from the SERDS data sets by fitting the latter to a series of derivative-shaped functions (in this case difference bands generated from Gaussian functions) of arbitrary frequency, amplitude, and width.

RESULTS

The low-temperature (10 K) near-infrared absorption spectra of wild-type, (M)L214H, and (M)L214H/(L)E104V RCs are compared in Figure 1. The absorption difference spectra (wild-type−mutant) are also shown in the figure. The Q_y-absorption features of both β-mutant RCs are distinguished from those of wild-type by the appearance of a new band in the 770−785 nm range and loss of the Q_y-absorption band of BPh_L near 763 nm. The new absorption feature observed for the β-mutant RCs has been attributed to the Q_y-band of β_L (*18*, *22*). Closer inspection of the spectral data reveals that the Q_y band of β_L in the (M)L214H/(L)-E104V mutant is slightly blue-shifted compared with that of β_L in the (M)L214H mutant (∼775 nm versus ∼780 nm). This shift is evidenced in the normal spectra by the fact that the Q_y band of the former mutant is much better distinguished from the Q_y bands of the accessory BChls (∼805 nm) than is the Q_y band of the latter mutant. In the difference absorption spectra, the slight blue shift of the Q_y band of the (M)L214H/(L)E104V versus (M)L214H mutant RCs appears as a narrowing of the negative-going difference feature. This latter feature is predominantly due to the absence of the Q_y band of BPh_L. The blue shift observed for the Q_y band of β_L in the (M)L214H/(L)E104V versus (M)L214H mutant RCs parallels that observed for the Q_y bands of BPh_L in wild-type versus single (L)E104V (*Rb. sphaeroides*) (*22*) and (L)E104L (*Rb. capsulatus*) (*54*, *55*) mutant RCs. The latter replacement removes the hydrogen bond to the C_9-keto group of BPh_L. The similar mutation-induced trends observed for the Q_y (and Q_x) absorption features in β-type versus normal-pigment composition RCs led Kirmaier et al. to suggest that glutamic acid L104 also forms a hydrogen bond with the C_9-keto group of β_L (*22*).

The likelihood that the Q_y-band of β_L occurs in the 770−785 nm region focused the RR studies on this spectral region. In particular, RR spectra were obtained in 5−10 nm excitation increments between 765 and 800 nm. The various exciting lines used to acquire RR data are marked by arrows on the near-infrared absorption spectrum of the (M)L214H/(L)E104V mutant shown in Figure 1. The RR data were acquired for the wild-type as well as both β-mutant RCs with these different exciting lines. These studies revealed two general characteristics of the RR scattering. First, with excitation in the 770−785 nm region, the RR intensity enhancements observed for both β-mutant RCs are at least 10 times larger than those observed for wild-type RCs. Accordingly, the RR spectra obtained for the β-type RCs with excitation in the 770−785 nm region are due almost exclusively to β_L with little or no interference from the accessory BChls. Second, with excitation at 800 nm, which probes the accessory BChls (*38*−*40*, *46*−*49*), the RR spectra obtained for the two β-mutant RCs are essentially identical to one another and identical to that of wild-type. Accordingly, substitution of BChl for BPh in the acceptor site does not alter the structural, vibrational, or electronic properties of the accessory BChls. This view is generally consistent with the optical absorption characteristics of the accessory BChls in the β-mutant RCs (*18*, *19*, *22*). Owing to the fact that the vibrational frequencies of analogous modes of $BChl_L$ and $BChl_M$ are very close and not resolved for each RC and among the different RCs, these cofactors of all three RCs will be denoted collectively as $BChl_{L,M}$ in the remainder of the text.

The high-frequency regions of the Q_y-excitation RR spectra of (M)L214H (λ_{ex} = 780 nm), (M)L214H/(L)E104V (λ_{ex} = 775 nm), and wild-type (λ_{ex} = 800 nm) RCs are shown in Figure 2. These exciting lines probe β_L of the two β-mutant RCs and $BChl_{L,M}$ of wild-type RCs (vide supra). In Figure 2, the top traces in each panel are the SERDS data; the second traces are the fits of the SERDS data; the third traces are the SERDS residuals (observed−fit); the bottom traces are the RR spectra reconstructed from the SERDS data. The relatively small residuals compared with the SERDS intensities are indicative of the excellent fidelity of the fits. Expanded views of the RR spectra in the 1575−1750-cm^{-1} range are shown in Figure 3. This spectral window encompasses of the region the carbonyl and certain ring-skeletal stretching modes (*27*−*38*).

The low-frequency regions of the Q_y-excitation RR spectra of (M)L214H (λ_{ex} = 780 nm), (M)L214H/(L)E104V (λ_{ex} =

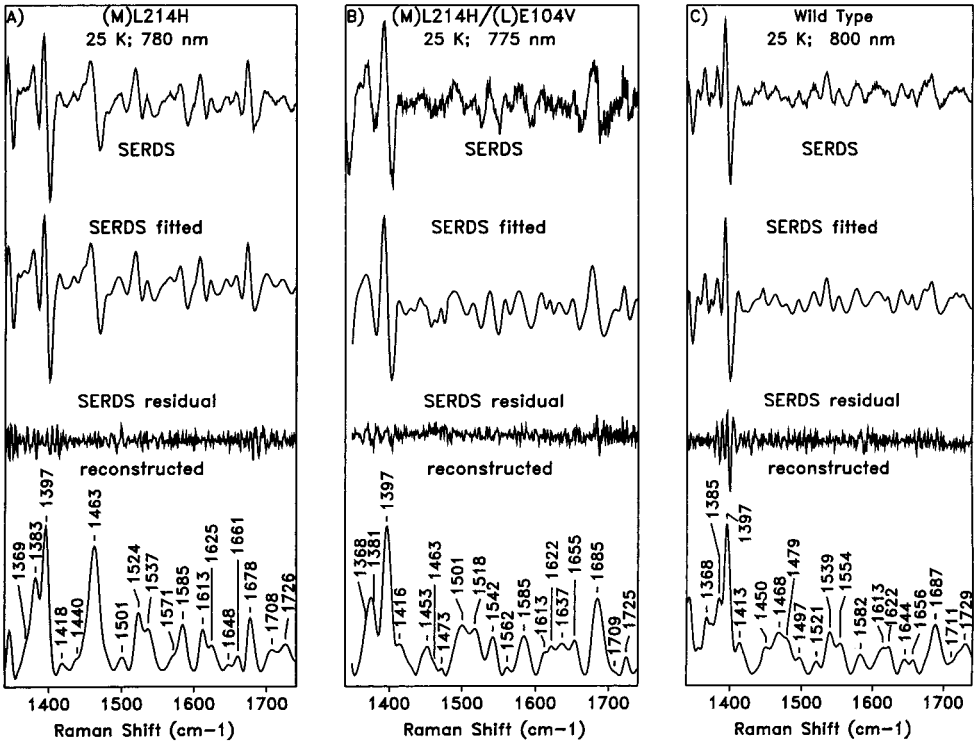

FIGURE 2: High-frequency regions of the Q_y-excitation RR spectra of (M)L214H (λ_{ex} = 780 nm), (M)L214H/(L)E104V (λ_{ex} = 775 nm), and wild-type (λ_{ex} = 800 nm) RCs. For the two β-mutant RCs, the spectra are due to β_L; for the wild-type RCs, the spectra are due to $BChl_{L,M}$ (see the text). The top traces in each panel are the SERDS data; the second traces are the fits of the SERDS data; the third traces are the SERDS residuals (observed−fit); the bottom trace is the RR spectrum reconstructed from the SERDS data.

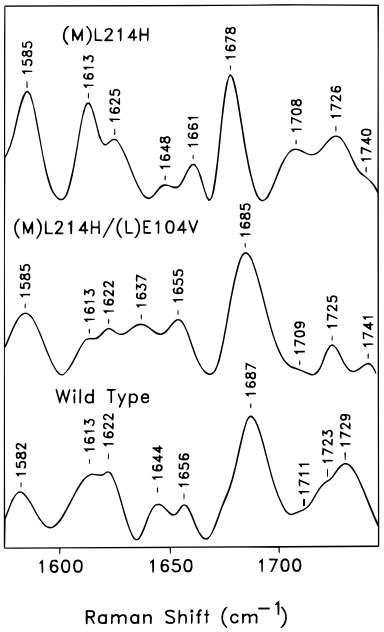

FIGURE 3: Expanded view of the Q_y-excitation RR spectra of (M)-L214H, (M)L214H/ (L)E104V, and wild-type RCs in the region of the carbonyl and high-frequency ring-skeletal stretching modes. The data are the same as the bottom traces of Figure 4.

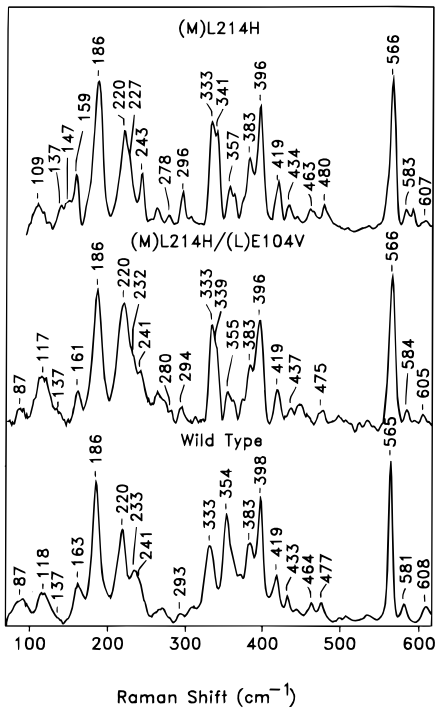

FIGURE 4: Low-frequency Q_y-excitation RR spectra of (M)L214H (λ_{ex} = 780 nm), (M)L214H/(L)E104V (λ_{ex} = 775 nm), and wild-type (λ_{ex} = 800 nm) RCs. For the two β-mutant RCs, the spectra are due to β_L; for the wild-type RCs, the spectra are due to $BChl_{L,M}$ (see text).

775 nm), and wild-type (λ_{ex} = 800 nm) RCs are shown in Figure 4. For the two β-mutant RCs, the spectra are due to β_L; for the wild-type RCs, the spectra are due to $BChl_{L,M}$. RR spectra were also acquired for the different RCs in the midfrequency range (650−1300 cm^{-1}) (not shown). The midfrequency RR data will not be considered in the characterization of β_L owing to the fact that the vibrational spectra of $BChl_{L,M}$ (or BChl *a* in general) have not been assigned in this region.

Inspection of Figures 2−4 (and the spectra obtained in the midfrequency region) reveals that Q_y-excitation of β_L results in a rich pattern of RR scattering throughout the 100−1750-cm^{-1} spectral region. This general feature of the RR scattering of β_L parallels that observed for $BChl_{L,M}$ (*48*, *49*)

Table 1: Frequencies (cm^{-1}) and Assignments[a] for Selected RR bands of β_L

description[b]	β_L (M)L214H	β_L (M)L214H/(L)E104V	$BChl_{L,M}$
$\nu C_9{=}O$	1678	1685	1687
$\nu C_{2a}{=}O$	1661	1655	1656
$\nu C_aC_m(\gamma)$, $\nu C_9{=}O$	1648	1637	1644
νC_bC_b(III), $\nu C_9{=}O$	1625	1622	1622
$\nu C_aC_m(\alpha,\beta,\gamma,\delta)$	1613	1613	1613
νC_bC_b(I), νC_aC_b(III)	1585	1585	1582
δC_bH	1463	1463	1468
νMgN_{his}	243	241	241
δC_bC_{alkyl}	227	232	233
δC_2C_{acetyl}	109	117	118

[a] Taken from refs 38−40. [b] Mode descriptions are as follows: ν = stretch, δ = in-plane deformation, γ = out-of-plane deformation. The designators C_a, C_b, C_m, I−IV, and α, β, γ, δ refer to Figure 5.

and BChl in films (*52*). The vibrations enhanced with Q_y-excitation include carbonyl, ring skeletal, and substituent modes (*30*, *36*, *38*−*49*, *52*). RR bands assignable to the $\nu C{=}O$ vibrations of the C_{2a}-acetyl and C_9-keto carbonyl groups are observed in the highest frequency spectral region, above 1650 cm^{-1} (*30*, *36*, *38*, *41*−*43*). RR bands assignable to stretching vibrations of the C_aC_m and unsaturated C_bC_b bonds of the macrocycle dominate the 1550−1650-cm^{-1} region (*38*). Bands arising from stretching vibrations of the C_aC_b and C_aN bonds of the macrocycle are the principal contributors to the 1300−1550-cm^{-1} region (*38*). RR bands due to deformations of the macrocycle and the peripheral substituent groups are the principal contributors to the lowest frequency region of the spectrum, below <500 cm^{-1} (*39*, *40*, *47*).

Comparison of the RR scattering characteristics of β_L in the two mutant RCs with one another and with those of $BChl_{L,M}$ reveals that the frequencies and number of RR bands observed in all spectral regions are very similar. In certain regions, the spectra of β_L and $BChl_{L,M}$ are essentially identical (particularly in the midfrequency region). Certain differences are observed between the intensities of analogous RR bands of the different cofactors. These differences arise in large part because the energies of the exciting lines relative to the Q_y-band origins of the cofactors are not identical for the spectra of the different RCs shown in Figures 2−4. Indeed, the exact position of the Q_y-band origins for β_L are difficult to locate owing to the fact that these absorptions overlap the Q_y bands of $BChl_{L,M}$ and BPh_M.

The fact that the RR signatures of β_L are so similar to those of $BChl_{L,M}$ permits assignment of the vibrational modes of the former cofactor by direct analogy to those of the latter. The rationale for the various vibrational assignments of $BChl_{L,M}$ has been previously discussed in detail and will not be reiterated here (*38*−*40*, *47*). The frequencies of selected high- and low-frequency RR bands of β_L are compared with those of $BChl_{L,M}$ in Table 1. The table is not intended to be comprehensive. Instead, the bands listed were chosen because they illustrate specific similarities or differences between the vibrational signatures of β_L in the two mutant RCs and/or between β_L and $BChl_{L,M}$. In addition, firm vibrational assignments are available for all of these modes (*38*−*40*). The normal mode descriptions are also included in the table. The various descriptors refer to the structure and labeling scheme for BChl shown in Figure 5.

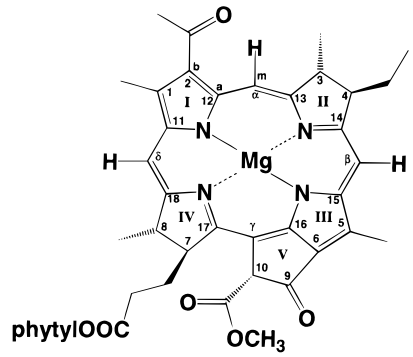

FIGURE 5: Structure and labeling scheme for BChl *a*.

DISCUSSION

The vibrational characteristics of β_L provide detailed insights into the structure and coordination geometry of the cofactor and the nature of its interaction with the protein matrix. These features in turn mediate the physicochemical properties of β_L and, hence, how the cofactor participates in the initial events of photoinduced charge separation. Two key questions concern the conformation and ligation of the β_L macrocycle and its orientation in the protein binding site. In the sections below, we discuss each of these issues in turn. We then conclude with a discussion of how the structure and local environment of β_L influence the photophysical properties of β-type RCs.

β_L-Macrocycle Conformation and Axial Ligation. The frequencies of the ring-skeletal and axial-ligand modes of the BChl macrocycle reflect the conformation of the ring and the nature and number of axial ligands to the Mg(II) ion (*37*−*40*, *44*, *45*, *56*). The vibrational characteristics of the ring-skeletal modes of $BChl_{L,M}$ provide a convenient benchmark for assessing these properties of β_L. $BChl_{L,M}$ are both five-coordinate with histidine serving as the axial ligand (*8*, *9*). In addition, the conformations of the $BChl_{L,M}$ macrocycles are similar to those of BChl in solution and, hence, reflect a nonperturbing protein environment (*38*). The appearance of the ring-skeletal stretching mode, $\nu C_aC_m(\alpha,\beta,\gamma,\delta)$, near 1613 cm^{-1} is the key vibrational signature for a pentacoordination geometry of BChl (*27*−*31*, *38*, *56*). The frequency of $\nu C_aC_m(\alpha,\beta,\gamma,\delta)$ does not, however, identify histidine as the axial ligand. In this regard, RR bands due to the stretching of the magnesium−histidine bond, νMgN_{his} have recently been identified in the Q_y-excitation spectra of $BChl_{L,M}$ near 240 cm^{-1} (*39*, *40*). Bands assignable to the doming vibration of the BChl core, γMg_{dome}, have also been identified near 137 cm^{-1} (*39*). The characteristics of the axial-ligand stretching and macrocycle doming vibrations of β_L are key to understanding the detailed structure of this cofactor.

Comparison of the vibrational signatures of the ring-skeletal/axial-ligand modes of β_L in the two different β-type RCs with one another and with those of $BChl_{L,M}$ reveals certain clear trends.

(1) The $\nu C_aC_m(\alpha,\beta,\gamma,\delta)$ modes of β_L in both β-type RCs occur near 1613 cm^{-1}, as is the case for $BChl_{L,M}$ (Figure 4, Table 1). The frequencies of the other ring-skeletal stretching vibrations of the two β_L cofactors are also similar to one another and similar to those of $BChl_{L,M}$. There are some minor differences among the frequencies for analogous modes; however, these differences are generally less than 5

cm^{-1}. The only ring-skeletal mode whose frequency falls out of this range is the highest frequency ring-skeletal mode of β_L in the (M)214H/(L)E104V mutant RCs which occurs near 1637 cm^{-1} compared with 1644 cm^{-1} for β_L in the (M)-214H mutant and 1648 cm^{-1} for $BChl_{L,M}$. The fact that the (L)E104V rather than that the (M)L214H mutation results in the only significant frequency shift of this ring-skeletal mode in conjunction with the fact that this mode contains substantial $\nu C_9{=}O$ character (Table 1) suggests that the shift of this mode for β_L in the double mutant reflects changes in C_9-keto group−protein interactions rather than macrocycle conformational differences. The issue of C_9-keto group−protein interactions will be discussed in more detail below.

(2) The β_L cofactors in both β-type RCs exhibit an identical pattern of RR bands in the 220−245-cm^{-1} region. This pattern is very similar to that observed for $BChl_{L,M}$. Consequently, the ∼242 cm^{-1} band of the β_L cofactors is assigned to the νMgN_{his} mode by analogy to that observed for $BChl_{L,M}$ (*39*, *40*). Indeed, if the Mg−His linkage were not present in β_L, a different spectral pattern would be expected in the 220−245-cm^{-1} region, as has been shown in previous RR studies of isolated BChl pigments in solid films wherein a keto oxygen atom of an adjacent BChl serves as the axial ligand (*39*, *52*). Finally, weak features are also observed for the β_L cofactors near 140 cm^{-1} which might be due to the γMg_{dome} vibrations. However, these features are so weak that this assignment is not certain.

Collectively, the vibrational characteristics of the ring-skeletal/axial-ligand modes of β_L in both β-type RCs unambiguously indicate that this cofactor is five-coordinate with histidine serving as the axial ligand. In addition, the conformation of the β_L macrocycle and the strength of the Mg−histidine bond are very similar to those of $BChl_{L,M}$. Accordingly, the structure/conformation of β_L is in every sense typical of that found for a five-coordinate BChl molecule in solution (*38*).

β_L-Macrocycle Orientation and Local Environment. The frequencies of the carbonyl stretching modes reflect the extent of hydrogen bonding between the different carbonyl groups on the BChl macrocycle and the amino acid residues of the protein (*27*−*35*, *41*−*46*). These interactions are determined by specific contacts as dictated by the orientation of the cofactor in the protein binding site. In addition, the frequencies of the carbonyl stretching modes are sensitive to the dielectric properties of the local environment (*57*−*59*). The carbonyl-stretching characteristics of both $BChl_{L,M}$ and BPh_L serve as benchmarks for assessing the environment around β_L. The vibrational signatures of $BChl_{L,M}$ indicate that both the C_9-keto and C_{2a}-acetyl groups are free of hydrogen bonds (*27*−*31*, *38*).[2] The latter group of BPh_L is also free of hydrogen bonds, whereas the former hydrogen bonds to glutamic acid L104 (*8*, *9*, *38*, *59*). Removal of the hydrogen bond to BPh_L via (L)E104L replacement (*Rb. capsulatus*) upshifts the frequency of $\nu C_9{=}O$ by ∼8 cm^{-1} (*59*). Despite this upshift, the frequency of the $\nu C_9{=}O$ mode of BPh_L is still significantly lower (by ∼14 cm^{-1}) than that of the analogous mode of BPh_M [whose C_9-keto group is free from hydrogen bonding (*8*, *9*, *28*−*30*, *38*)]. The lower than expected frequency of the $\nu C_9{=}O$ mode of BPh_L has been attributed to a difference in the dielectric properties on the L- versus M-side of the protein in the region of the BPh cofactors (*58*), as indicated by Stark-effect measurements on RCs (*60*). The (L)E104L replacement also affects the frequency of the $\nu C_{2a}{=}O$ mode of BPh_L in wild-type RCs (*44*). In particular, this mode downshifts by ∼4 cm^{-1}. The origin of this downshift is not certain.

Comparison of the vibrational signatures of the $\nu C_9{=}O$ and $\nu C_{2a}{=}O$ modes of β_L in the (M)L214H versus (M)-L214H/(L)E104V RCs reveals a pattern which is very similar to that observed for BPh_L in wild-type versus (L)E104L RCs (*44*,*59*) (Figures 2 and 3, Table 1). In particular, the $\nu C_9{=}O$ and $\nu C_{2a}{=}O$ modes of β_L in the (M)L214H RCs occur at 1678 and 1661 cm^{-1}, respectively. The addition of the (L)-E104V replacement upshifts the former mode to 1685 cm^{-1} and downshifts the latter to 1655 cm^{-1}. Accordingly, both the direction and magnitude of the (L)E104V/L-induced frequency shifts of the carbonyl modes of β_L and BPh_L are essentially identical. In the double β-mutant, the frequencies of the $\nu C_9{=}O$ and $\nu C_{2a}{=}O$ modes of β_L (1685 and 1655 cm^{-1}, respectively) are also very similar to those of the analogous modes of $BChl_{L,M}$ (1687 and 1656 cm^{-1}, respectively).

The (L)E104V-mutation-induced shift of the $\nu C_9{=}O$ mode of β_L indicates that the C_9-keto group of this cofactor in the (M)L214H mutant is hydrogen bonded to the glutamic acid L104, as is also the case for BPh_L. The similar magnitudes of the frequency upshifts of the $\nu C_9{=}O$ modes of β_L and BPh_L resulting from the (L)E104V/L replacements further suggest that the strengths of the hydrogen bonds to the two different cofactors are nearly identical. The vibrational signatures of the C_{2a}-acetyl groups of β_L in both β-type RCs indicate that these groups are free of hydrogen bonds, again paralleling the behavior of BPh_L. Finally, the (L)E104V/L replacement relaxes the perturbation on the C_{2a}-acetyl groups of β_L and BPh_L in a similar fashion. The nature of the perturbation on the C_{2a}-acetyl group is not clearly delineated by the behavior of the $\nu C_{2a}{=}O$ modes and could involve either an electronic or a structural effect (or both). However, as will be discussed further below, other vibrational characteristics of β_L give clear evidence that the perturbation is structural in origin.

The vibrational characteristics of the deformations of the peripheral substituent (both carbonyl and other) groups provide an additional monitor of the interactions between the BChl macrocycle with the protein matrix (*52*, *61*−*63*). These vibrations principally contribute to the very low-frequency region of the spectrum (<250 cm^{-1}), with the exception of hydrogenic modes which occur at much higher frequencies (700−1500 cm^{-1}). Detailed vibrational assignments for the substituent deformations have only recently become available (*38*, *39*).

Comparison of the very low-frequency (<250 cm^{-1}) vibrational signatures of β_L in the two β-type RCs reveals many similarities with two clear exceptions (Figure 4, Table 1). In the case of the (M)L214H mutant, the deformation of the C_{2a}-acetyl group with respect to the bacteriochlorin ring, δC_2C_{acetyl}, is at ∼109 cm^{-1} and the deformation involving the C_b-alkyl groups on rings I, II, and IV, δC_bC_{alkyl},

[2] The X-ray structure of *Rb. sphaeroides* shows water molecules in close proximity to the C_9-keto groups of $BChl_{L,M}$ (*8*). As a consequence, it has been suggested that these water molecules are hydrogen bonded to the C_9-keto groups of both cofactors. Regardless, the vibrational signatures for the $\nu C_9{=}O$ modes are not commensurate with the formation of hydrogen bonds (*28*−*33*, *38*). In particular, the frequencies of the $\nu C_9{=}O$ modes of $BChl_{L,M}$ are very similar to those of isolated BChl in a low dielectric, non-hydrogen-bonding solvent.

is at ~227 cm^{-1}. These frequencies are distinctly lower than those of the analogous vibrations of β_L in the (M)L214H/(L)E104V mutant, for which δC_2C_{acetyl} is at ~117 cm^{-1} and δC_bC_{alkyl} is at ~232 cm^{-1}. On the other hand, the frequencies of the δC_2C_{acetyl} and δC_bC_{alkyl} modes of β_L in the latter RC are essentially identical to those of the analogous vibrations of $BChl_{L,M}$, which occur at ~118 and ~232 cm^{-1}, respectively. A similar trend is observed in the RR intensity enhancement patterns of the hydrogenic deformations of the alkyl substituents, δC_bH, which occur near 1463 cm^{-1} (Figure 4) (*38*). In particular, the δC_bH mode of β_L is very strongly enhanced in the (M)L214H mutant. In contrast, the intensity of this mode is significantly attenuated for β_L in the L(M214)/(L)E104V mutant and is qualitatively more similar to that observed for $BChl_{L,M}$.

Collectively, the vibrational characteristics of the $\nu C_9{=}O$ and $\nu C_{2a}{=}O$ modes strongly suggest that the location and orientation of β_L in the protein binding site is similar to that of BPh_L. Indeed, it is difficult to imagine how cofactor−protein interactions involving carbonyl groups on opposite sides of the macrocycle could be preserved if β_L and BPh_L were not positioned and oriented in an identical fashion in the protein binding site. This view is in general accord with that indicated by preliminary X-ray crystallographic data for (M)L214H RCs (*25*). The fact that the $\nu C_9{=}O$ and $\nu C_{2a}{=}O$ frequencies of β_L in the double β-mutant are similar to those of $BChl_{L,M}$ further suggests that the strength of the local electric field in the vicinity of the C_9-keto and C_{2a}-acetyl groups of β_L is similar to that near these groups of $BChl_{L,M}$. [The $\nu C_9{=}O$ and $\nu C_{2a}{=}O$ frequencies of $BChl_{L,M}$ should reflect primarily electric field effects owing to the fact that these groups' cofactors are free of hydrogen bonds (*8*, *9*, *27*−*31*, *38*).] Finally, the vibrational characteristics of the $\nu C_{2a}{=}O$ modes, in conjunction with those of the δC_2C_{acetyl}, δC_bC_{alkyl}, and δC_bH modes, reinforce the view that the hydrogen-bonding interaction between the C_9-keto group and glutamic acid L104 influences the exact position of β_L and BPh_L in the protein binding site. This interaction in turn induces secondary interactions between the peripheral substituents (C_{2a}-acetyl and C_b-alkyl groups) and the protein matrix.

Implications for the Photophysical Properties β-Type RCs. The vibrational characteristics of β_L indicate that its conformation and ligation state are very similar to those of $BChl_{L,M}$. These features in turn suggest that the intrinsic redox properties of β_L must be qualitatively similar to those of the $BChl_L$. It must be stressed; however, that the local environment around β_L and $BChl_{L,M}$ cannot be completely identical, otherwise the Q_y absorption bands for the two types of BChls in the RC would not be separated by 20−25 nm (~400 cm^{-1}). The detailed redox properties of β_L versus $BChl_L$ are clearly important for determining the exact contribution of $P^+\beta_L^-$ versus $P^+BChl_L^-$ to the initial charge-separated intermediate P^+I^- (*22*, *23*). Accordingly, the general similarities between the physicochemical properties of β_L and $BChl_L$ suggests that the states $P^+\beta_L^-$ and $P^+BChl_L^-$ must both make substantial (but not necessarily equal) contributions to P^+I^-. This view leads to the assessment that P^+I^- is most aptly described as a thermal/quantum admixture of $P^+\beta_L^-$ and $P^+BChl_L^-$. This general picture is in accord with the conclusions reached by Kirmaier et al. (*22*, *23*).

The intrinsically similar properties of β_L and $BChl_L$ indicate that any differences which do arise must be linked to rather specific features of the binding sites of the two cofactors. The interaction with glutamic acid L104 in the acceptor site is clearly implicated as the key structural feature responsible for the differential pigment−protein interactions in the two sites. The fact that both β_L and BPh_L experience many of the same perturbations reinforces the view that the perturbations induced by the L104 glutamic acid are a general feature of the binding site.

The secondary perturbations induced by the C_9-keto/L104 glutamic acid interaction may partially explain certain anomalous features of the photophysical properties of (M)-L214H versus (M)L214H/(L)E104V RCs. In particular, the free-energy gaps between P* and P^+I^- of the former and latter RCs have been estimated to be ~75 and ~50 mV, respectively (*23*). The smaller free-energy gap of the double β-mutant is expected because removal of the hydrogen bond to the C_9-keto group increases the redox potential of the pigment (*64*, *65*), thus moving P^+I^- closer to P*. Nevertheless, the magnitude of the difference between the free-energy gaps of single versus double β-type RCs is considerably smaller than expected. In this regard, studies of other hydrogen-bonding mutant RCs have shown that each hydrogen bond to a C_9-keto or C_{2a}-acetyl group is worth 50−80 mV in redox potential (*64*, *65*). In comparison, the difference in the P^*/P^+I^- free-energy gaps for the (M)L214H versus (M)L214H/(L)E104V RCs is only ~25 mV.

The influence of the L104 glutamic acid on the C_2-acetyl group could account for the attenuated value of the P^*/P^+I^- free-energy difference in single versus double β-mutant RCs. In particular, the significant frequency difference of the δC_2C_{acetyl} modes of β_L in the single versus double β-mutants suggests that the torsional angles of the C_{2a}-acetyl groups are different. The lower $\nu C_{2a}{=}O$ frequency for β_L in the double mutant is qualitatively consistent with rotation of the C_{2a}-acetyl group to a position which affords increased conjugation of this group into the π-electron system of the macrocycle. This would tend to lower the redox potential of β_L (*66*, *67*) and would partially compensate for the increased redox potential resulting from removal of the hydrogen bond via the (L)E104V replacement. The net result would be a P^*/P^+I^- free-energy gap which is smaller than nominally expected.

The detailed aspects of the factors which control the free energy gaps in the β-type RCs are most likely more complicated than described above (*22*, *23*). Regardless of these details, the behavior exhibited by the β_L pigments illustrates that a variety of factors must be considered when assessing the effects of genetic alterations or when designing genetic manipulations intended to achieve certain effects. The full body of pigment−protein interactions and their influence on the structural and electronic properties of the cofactors must be considered in order to develop a model which properly accounts for the complete spectrum of photophysical characteristics of β-type (or any other mutant) RCs.

ACKNOWLEDGMENT

We thank Dr. D. Holten for insightful discussions and Dr. V. Palaniappan for assistance in initiating the Q_y-excitation RR studies.

REFERENCES

1. Kirmaier, C., and Holten, D. (1987) *Photosynth. Res. 113*, 225−260.
2. Friesner, R. A., and Won, Y.(1989) *Biochim. Biophys. Acta 977*, 99−122.
3. Breton, J., and Verméglio, A., Eds. (1992) *NATO Ser. A*, Vol. *237*.
4. Deisenhofer, J., and Norris, J. R., Eds. (1993) *The Photosynthetic Reaction Center*, Vol. II, Academic, San Diego.
5. Blankenship, R. E., Madigan, M. T., Bauer, C. E., Eds. (1995) *Anoxygenic Photosynthetic Bacteria*, pp 503−708, Kluwer Academic Publishers, Dordrect, The Netherlands.
6. Michel-Beyerle, M. E., Ed. (1996) *The Reaction Center of Photosynthetic Bacteria*, Springer, Berlin-Heidelberg.
7. Deisenhofer, J., and Michel, H. (1991) *Annu. Rev. Biophys. Biophys. Chem. 20*, 247−266.
8. Ermler, U., Fritzsch, G., Buchanan, S., and Michel, H. (1994) *Structure 2*, 925−936.
9. Deisenhofer, J., Epp, O., Sinning, I., and Michel, H. (1995) *J. Mol. Biol. 246*, 429−457.
10. Allen, J. P., Feher, G., Yeates, T. O., Komiya, H., and Rees, D. C. (1987), *Proc. Natl. Acad. Sci. U.S.A. 84*, 5730−5734.
11. Yeates, T. O., Komiya, H., Chirino, A., Rees, D. C., Allen, J. P., and Feher, G. (1988) *Proc. Natl. Acad. Sci. U.S.A. 85*, 7993−7997.
12. Allen, J. P., Feher, G., Yeates, T. O., Komiya, H., and Rees, D. C. (1988) *Proc. Natl. Acad. Sci. U.S.A. 85*, 8487−8491
13. Chang, C.-H., Tiede, D., Tang, J., Smith, U., Norris, J., Schiffer, M. (1986) *FEBS Lett. 205*, 82−86.
14. Chang, C.-H., El-Kabbani, O., Tiede, D., Norris, J., and Schiffer, M. (1991) *Biochemistry 30*, 5352−5360.
15. El-Kabbani, O., Chang, C.-H., Tiede, D., Norris, J., and Schiffer, M. (1991) *Biochemistry 30*, 5361−5369.
16. Kirmaier, C., Holten, D., and Parson, W. W. (1985) *Biochim. Biophys. Acta 810*, 49−61.
17. For a recent review of electron-transfer in mutant RCs, see Woodbury, N. W., and Allen, J. P. in ref 5, pp 527−557.
18. Kirmaier, C., Gaul, D., DeBey, R., Holten, D., and Schenck, C. C. (1991) *Science 251*, 922−927.
19. Heller, B. A., Holten, D., and Kirmaier, C. (1995) *Biochemistry 34*, 5294−5302.
20. For a recent review of RCs containing modified tetrapyrroles, see: Scheer, H., and Gartwich, G. in ref 5, pp 649−663.
21. Felton, R. H. (1978) in *The Porphyrins* (Dolphin, D., Ed.) Vol. V, pp 53−126, Academic, New York.
22. Kirmaier, C., Laporte, L., Schenck, C. C., and Holten, D. (1995) *J. Phys. Chem. 99*, 8903−8909.
23. Kirmaier, C., Laporte, L., Schenck, C. C., and Holten, D. (1995) *J. Phys. Chem. 99*, 8910−8917.
24. Laporte, L., Kirmaier, C., Schenck, C. C., and Holten, D. (1995) *Chem. Phys. 197*, 225−237.
25. Chirino, A. J., Lous, E. J., Huber, M., Allen, J. P., Schenck, C. C., Paddock, M. L., Feher, G., and Rees, D. C. (1994) *Biochemistry 33*, 4584−4593.
26. Heller, B. A., Holten, D., and Kirmaier, C. (1995) *Science 269*, 940−945.
27. Lutz, M. (1984) *Adv. Infrared Raman Spectrosc. 11*, 211−300.
28. Lutz, M., and Robert, B. (1988) In *Biological Applications of Raman Spectroscopy* (Spiro, T. G., Ed.) Vol. 3, pp 347−411, Wiley, New York.
29. Lutz, M., and Mäntele, W. (1991) In *Chlorophylls* (Scheer, H., Ed.) pp 855−902, CRC Press: Boca Raton, FL.
30. Lutz, M. (1995) *Biospectrosc. 1*, 313−327.
31. Robert, B., and Lutz, M. (1988) *Biochemistry 27*, 5108−5114.
32. Mattioli, T. A., Hoffman, A., Robert, B., Schrader, B., and Lutz, M. (1991) *Biochemistry 30*, 4648−4654.
33. Mattioli, T. A., Hoffman, A., Sockalingum, D. G., Robert, B., and Lutz, M. (1993) *Spectrochim. Acta 49A*, 785−799.
34. Feiler, U., Albouy, D., Mattioli, T. A., Lutz, M., and Robert, B. (1994) *Biochemistry 33*, 7594−7599.
35. Mattioli, T. A. (1995) *J. Mol. Struct. 347*, 459−466.
36. Bocian, D. F., Boldt, N. J., Chadwick, B. A., and Frank, H. A. (1987) *FEBS Lett. 214*, 92−96.
37. Peloquin, J. M., Violette, C. A., Frank, H. A., and Bocian, D. F. (1990) *Biochemistry 29*, 4892−4898.
38. Palaniappan, V., Martin, P. C., Chynwat, V., Frank, H. A., and Bocian, D. F. (1993) *J. Am. Chem. Soc. 115*, 12035−12049.
39. Czarnecki, K., Diers, J. R., Chynwat, V., Erickson, J. P., Frank, H. A., and Bocian, D. F. (1997) *J. Am. Chem. Soc. 119*, 415−426.
40. Czarnecki, K., Chynwat, V., Erickson, J. P., Frank, H. A., and Bocian, D. F. (1997) *J. Am. Chem. Soc. 119*, 2594−2595.
41. Wachtveitl, J., Farchaus, J. W., Das, R., Lutz, M., Robert, B., and Mattioli, T. A. (1993) *Biochemistry 32*, 12875−12886.
42. Mattioli, T. A., Williams, J. C., Allen, J. P., and Robert, B. (1994) *Biochemistry 33*, 1636−1643.
43. Mattioli, T. A., Lin, X., Allen, J. P., and Williams, J. C. (1995) *Biochemistry 43*, 6142−6152.
44. Peloquin, J. M., Bylina, E. J., Youvan, D. C., and Bocian, D. F. (1990) *Biochemistry 29*, 8417−8424.
45. Peloquin, J. M., Bylina, E. J., Youvan, D. C., and Bocian, D. F. (1991) *Biochim. Biophys. Acta 1056*, 85−88.
46. Palaniappan, V., and Bocian, D. F. (1995) *Biochemistry 34*, 11106−11116.
47. Palaniappan, V., Schenck, C. C., and Bocian, D. F. (1995) *J. Phys. Chem. 99*, 17049−17058.
48. Cherepy, N. J., Shreve, A. P., Moore, L. J., Franzen, S., Boxer, S. G., and Mathies, R. A. (1994) *J. Phys. Chem. 98*, 6023−6029.
49. Cherepy, N. J., Holzwarth, A., and Mathies, R. A.(1995) *Biochemistry 34*, 5288−5293.
50. Nagarajan, V., Parson, W. W., Gaul, D., and Schenck, C. C. (1990) *Proc. Natl. Acad. Sci. U.S.A. 87*, 7888−7892.
51. Yu, N.-T., and Srivastava, R. B.(1980) *J. Raman Spectrosc. 9*, 166−171.
52. Diers, J. R., and Bocian, D. F. (1995) *J. Am. Chem. Soc. 117*, 6629−6630.
53. Shreve, A. P., Cherepy, N. J., Mathies, R. A. (1992) *Appl. Spectrosc. 46*, 707−711.
54. Bylina, E. J., Kirmaier, C., McDowell, L. , Holten, D., and Youvan, D. C. (1988) *Nature 336*, 182−184.
55. Breton, J., Bylina, E. J., and Youvan, D. C. (1989) *Biochemistry 28*, 6423−6430.
56. Koyama, Y., Umemoto, Y., and Akamatsu, A. (1986) *J. Mol. Struct. 146*, 273−287.
57. Callahan, P. M., and Cotton, T. M. (1987) *J. Am. Chem. Soc. 109*, 7001−7007.
58. Krawczyk, S. (1989) *Biochim. Biophys. Acta 976*, 140−149.
59. Palanniappan, V., and Bocian, D. F. (1995) *J. Am. Chem. Soc. 117*, 3647−3648.
60. Stefan, M., Lao, K., and Boxer, S. G. (1994) *Science 264*, 810−816.
61. Diers, J. M., Zhu, Y., Blankenship, R. E., and Bocian, D. F. (1996) *J. Phys. Chem. 100*, 8573−8579.
62. Choi, S., and Spiro, T. G. (1983) *J. Am. Chem. Soc. 105*, 3683−3692.
63. Li, X.-Y., Czernuszewicz, R. S., Kincaid, J. R., and Spiro, T. G. (1989) *J. Am. Chem. Soc. 111*, 7012−7023.
64. Williams, J. C., Alden, R. G., Murchison, H. A., Peloquin, J. M., Woodbury, N. W., and Allen, J. P. (1992) *Biochemistry 31*, 11029−11037.
65. Lin, X., Murchison, H. A., Nagarjan, V., Parson, W. W., William, J. C., and Allen, J. P. (1994) *Proc. Natl. Acad. Sci. U.S.A. 91*, 10265−10268,
66. Muegge, I., Apostolakis, J., Ermler, U., Fritzsch, G., Lubitz, W., and Knapp, E. W. (1996) *Biochemistry 35*, 8359−8370.
67. Apostolakis, J., Muegge, I., Ermler, U., Fritzsch, G., and Knapp, E. W. (1996) *J. Am. Chem. Soc. 118*, 3743−3752.

BI971600M